Electronic Supplementary Information
for

Double helices of dissymmetrical α,α'-disubstituted tripyrrins.

Yui Fukuda,[a] Yuki Akamatsu,[a] Masataka Umetani,[a] Koki Kise,[a] Kenichi Kato,[a] Atsuhiro Osuka[a] and Takayuki Tanaka*[a,b]

[a] *Department of Chemistry, Graduate School of Science, Kyoto University.*
[b] *Department of Molecular Engineering, Graduate School of Engineering, Kyoto University.*

Contents

1. Experimental Procedure

General information

Commercially available solvents and reagents were used without further purification, unless otherwise noted. Dry acetonitrile was purchased from FUJIFILM Wako Pure Chemical Corporation. Dry THF was obtained by passing through alumina under N_2 in a solvent purification system. The spectroscopic grade solvents were used for all the spectroscopic studies. Silica gel column chromatography was performed on Wakogel C-300. UV/Vis absorption spectra were recorded on a Shimadzu UV-3600 spectrometer. ^{1}H, ^{13}C and ^{19}F NMR spectra were recorded on a JEOL ECA-600 spectrometer (operating as 600 MHz for ^{1}H, 151 MHz for ^{13}C and 565 MHz for ^{19}F) using the residual solvent as the internal reference for ^{1}H (δ = 7.26 ppm in $CDCl_3$, δ = 2.50 ppm in DMSO-d_6 and δ = 1.43 ppm in cyclohexane-d_{12}) and for ^{13}C (δ = 77.16 ppm in $CDCl_3$) and hexafluorobenzene as an external reference for ^{19}F (δ = –162.9 ppm in $CDCl_3$). High-resolution atmospheric-pressure-chemical-ionization time-of-flight mass-spectrometry (HR-APCI-TOF-MS) was recorded on a BRUKER micrOTOF model using positive ion mode. Recycling preparative GPC–HPLC was performed on a Japan Analytical Industry LaboACE LC-5060 equipped with JAIGEL-1HR (Φ20 mm, flow rate; 10 mL/min). Single-crystal X-ray diffraction analysis data were collected at –180 °C with a Rigaku XtaLAB P200 by using graphite monochromated Cu-K_α radiation (λ = 1.54187 Å). The structures were solved by direct methods (SHELXT-2014/5)[S1] and refined with full-matrix least-square technique (SHELXL-2014/7).[S2] All calculations were carried out using the *Gaussian 16* program.[S3]

1-(3,5-bis(trifluoromethyl)anilino)-14-bromo-5,10-diphenyltripyrrin (4)
To a mixture of α,α'-dibromotripyrrin **3** (266 mg, 0.50 mmol), dry THF (65 mL) and dry acetonitrile (65 mL) was added 3,5-bis(trifluoromethyl)aniline (83 μL, 0.50 mmol), and the resulting solution was stirred at 55 °C for 24 h under N_2. After quenching with water, the organic layer was extracted with ethyl acetate. The organic fraction was washed with water and dried over anhydrous Na_2SO_4. The solvent was evaporated to dryness. The crude product was purified by Gel Permeation Chromatography (GPC) column using distillated THF as eluent to afford blue solid of **4** (216 mg, 0.32 mmol) in 64% yield.
HR APCI-TOF-MS: m/z = 679.0901 (calcd. for $[C_{34}H_{22}{}^{79}BrF_6N_4]^+$: $[M+H]^+$, m/z = 679.0927)

1-(3,5-bis(trifluoromethyl)anilino)-14-(4-methoxyanilino)-5,10-diphenyltripyrrin (2a)
A mixture of **4** (50 mg, 0.074 mmol) and *p*-methoxyanilinium chloride (12 mg, 0.074 mmol) in dry THF (15 mL) and dry acetonitrile (15 mL) was stirred at 55 °C for 10 h under Ar. The solution was extracted with ethyl acetate. The organic fraction was washed with aqueous $NaHCO_3$ solution and dried with anhydrous Na_2SO_4 and concentrated under reduced pressure. The crude product was purified by column chromatography on silica gel (C-400: dichloromethane/*n*-hexane = 2/1 to 10/1) and recrystallization from dichloromethane/*n*-hexane to give **2a** (41 mg, 0.057 mmol) as blue solids in 77% yield.
HR APCI-TOF-MS: m/z = 722.2313 (calcd. for $[C_{41}H_{30}F_6N_5O]^+$; $[M+H]^+$, m/z = 722.2349)

1-(3,5-bis(trifluoromethyl)anilino)-14-(3,5-di-*tert*-butylanilino)-5,10-diphenyltripyrrin (2b)
A mixture of **4** (34.0 mg, 0.050 mmol) and 3,5-di-*tert*-butylanilinium chloride (12.1 mg, 0.050 mmol) in dry THF (10 mL) and dry acetonitrile (10 mL) was stirred at room temperature for 25 h under Ar. The solution was extracted with ethyl acetate and the organic fraction was washed with water and brine. The organic fraction was dried with anhydrous Na_2SO_4 and concentrated under reduced pressure. The crude product was purified by column chromatography on silica gel (Wakosil: dichloromethane/*n*-hexane = 1/1 to 2/1) to give **2b** (38.3 mg, 0.048 mmol) as blue solids in 95% yield.
HR APCI-TOF-MS: m/z = 804.3461 (calcd. for $[C_{48}H_{44}F_6N_5]^+$; $[M+H]^+$, m/z = 804.3495)

2. NMR Spectra

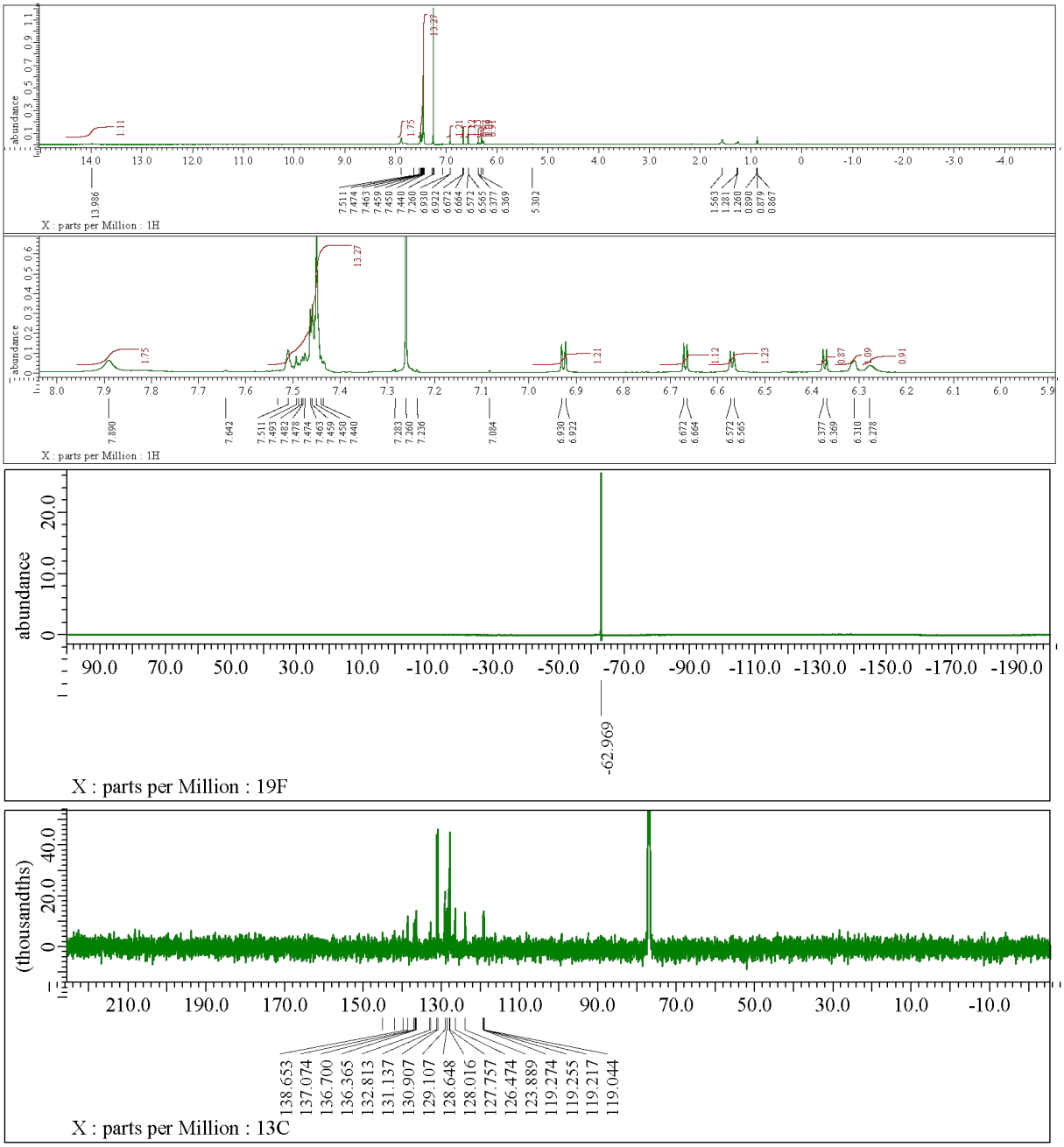

Figure S2-1. ^{1}H, ^{13}C and ^{19}F NMR spectra of **4** at 25 °C in $CDCl_3$.

Compound data of **4** in $CDCl_3$

^{1}H-NMR (600 MHz, $CDCl_3$) δ 13.99 (s, 1H, NH), 7.89 (s, 1H, NH), 7.53-7.43 (m, 13H, Ph-H+Ar-H), 6.93 (d, J = 4.6 Hz, 1H, β-H), 6.67 (d, J = 4.6 Hz, 1H, β-H), 6.57 (d, J = 4.6 Hz, 1H, β-H), 6.37 (d, J = 4.6 Hz, 1H, β-H), 6.31 (s, 1H, β-H) and 6.28 (s, 1H, β-H) ppm; ^{19}F-NMR (565 MHz, $CDCl_3$) δ –63.0 ppm; ^{13}C-NMR (151 MHz, $CDCl_3$) δ 145.0, 141.9, 139.9, 138.7, 137.1, 136.7, 136.6, 136.4, 133.0, 132.8, 131.1, 130.9, 129.1, 128.6, 128.0, 127.8, 126.5, 123.9, 119.3, 119.3, 119.3, 119.2, 119.1 and 119.0 ppm

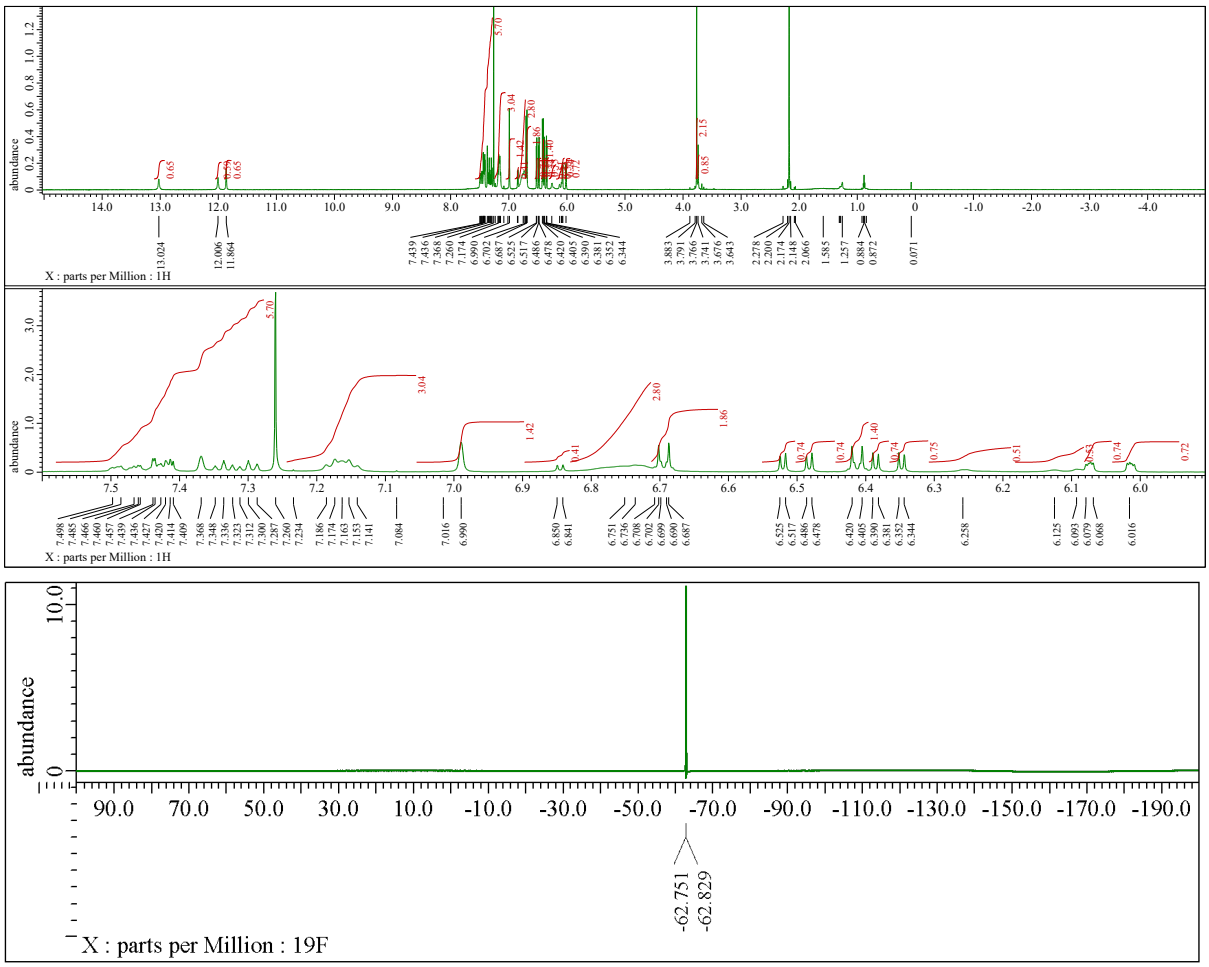

Figure S2-2. ^{1}H and ^{19}F NMR spectra of **2a** in $CDCl_3$ at 25 °C.

Compound data of **2a** in $CDCl_3$

^{1}H-NMR (600 MHz, $CDCl_3$) δ 13.02 (s, 2H, dimer NH), 12.01 (s, 2H, dimer NH), 11.86 (s, 2H, dimer NH), 7.50-7.29 (m, 4H+13H, dimer and monomer Ph+Ar-H), 7.19-7.14 (m, 8H, dimer Ph), 6.99 (s, 4H, dimer Ar-H), 6.85 (d, J = 5.0 Hz, 2H, monomer MeO-C_6H_4), 6.83-6.70 (br, 8H, dimer Ph), 6.69 (d, J = 8.7 Hz, 4H, dimer MeO-C_6H_4), 6.52 (d, J = 5.0 Hz, 2H, dimer β-H), 6.48 (d, J = 4.6 Hz, 2H, dimer β-H), 6.42 (s, 2H, dimer MeO-C_6H_4), 6.41 (s, 2H, dimer MeO-C_6H_4), 6.38 (d, J = 5.0 Hz, 2H, dimer β-H), 6.36 (d, J = 4.6 Hz, 2H, dimer β-H), 6.25 (br, 1H, monomer β-H), 6.13 (br, 1H, monomer β-H), 6.09 (br, 1H, monomer β-H), 6.07 (br, 2H, dimer β-H), 6.01 (br, 2H, dimer β-H), 3.77 (s, 6H, dimer OCH_3), 3.74 (s, 3H, monomer OCH_3) (Some signals of the monomer were not observed because of their broadness.); ^{19}F-NMR (565 MHz, $CDCl_3$) δ –62.75 and –62.83 ppm

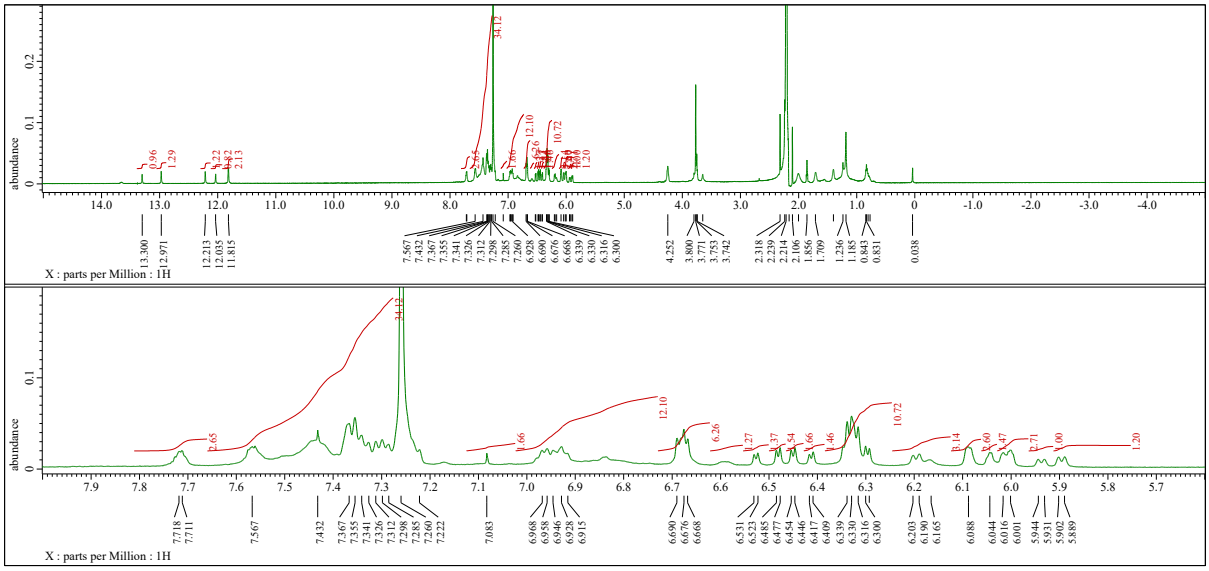

Figure S2-3. ^{1}H NMR spectra of **2a** in $CDCl_3$ at –60 °C.

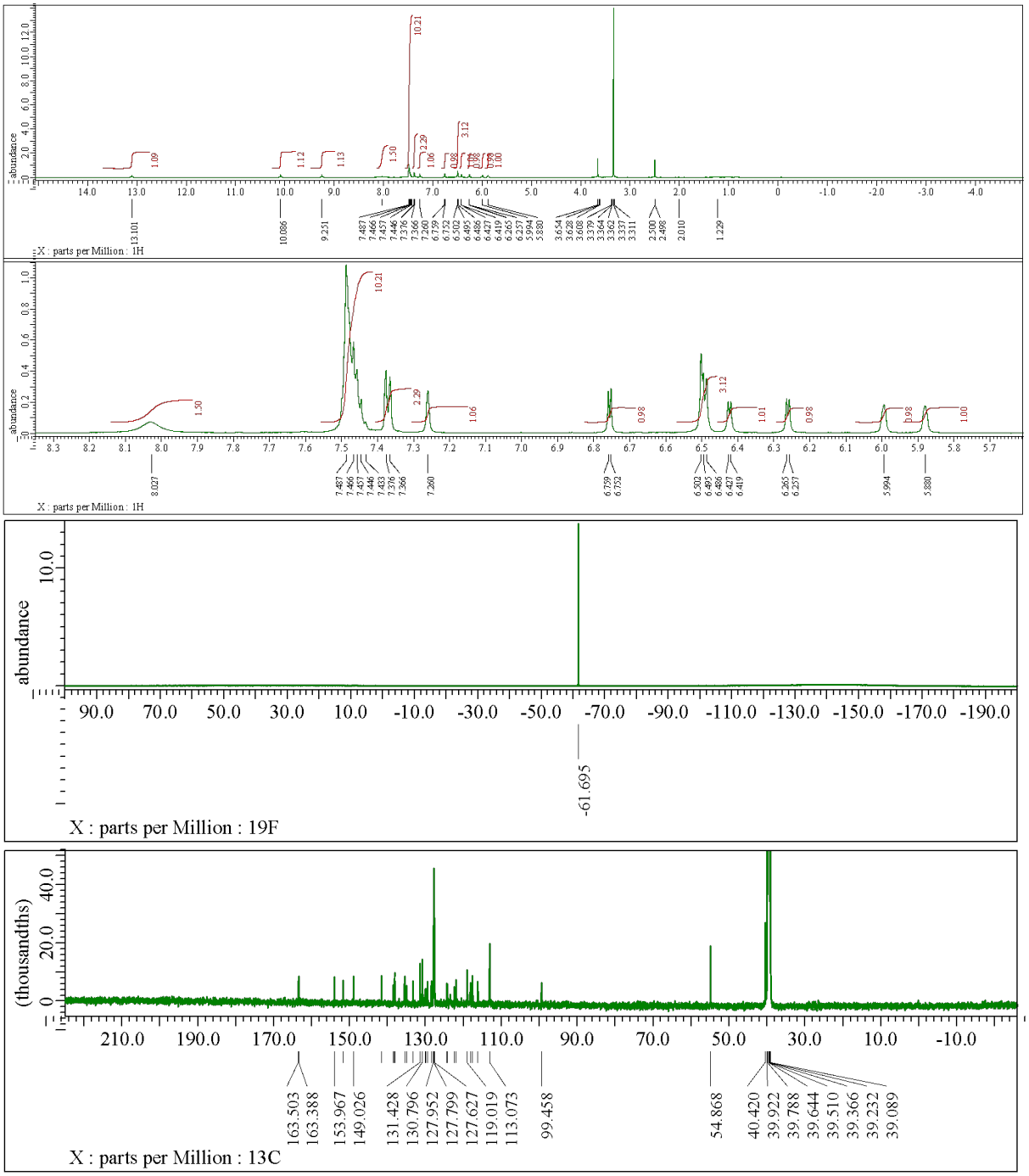

Figure S2-4. ^{1}H, ^{19}F and ^{13}C NMR spectra of **2a** in DMSO-d_6 at 25 °C.

Compound data of **2a** in DMSO-d_6 at 25 °C

^{1}H-NMR (600 MHz, DMSO-d_6) δ 13.10 (s, 1H, NH), 10.09 (s, 1H, NH), 9.25 (s, 1H, NH), 8.02 (br, 2H, Ar-H), 7.53-7.43 (m, 10H, Ph), 7.37 (d, J = 6.0 Hz, 2H, MeO-C$_6$H$_4$), 7.26 (s, 1H, Ar-H), 6.76 (d, J = 4.6 Hz, 1H, β-H), 6.50 (m, 3H, MeO-C$_6$H$_4$+β-H), 6.43 (d, J = 4.6 Hz, 1H, β-H), 6.26 (d, J = 4.6 Hz, 1H, β-H), 5.99 (s, 1H, β-H), 5.88 (s, 1H, β-H) and 3.65 (s, 3H, OCH$_3$) ppm; ^{19}F-NMR (600 MHz, DMSO-d_6) δ –61.70 ppm. ^{13}C-NMR (151 MHz, DMSO-d_6) δ 163.5, 163.4, 154.0, 151.8, 149.0, 141.6, 138.5, 138.2, 138.1, 135.5, 135.5, 135.0, 133.3, 131.4, 130.8, 130.2, 129.9, 129.5, 128.4, 128.0, 127.8, 127.6, 124.3, 124.2, 122.4, 122.0, 119.0, 118.2, 117.7, 116.2, 113.1, 99.5 and 54.9 ppm (Some signals were not observed because of their broadness or overlapping with the major signals.)

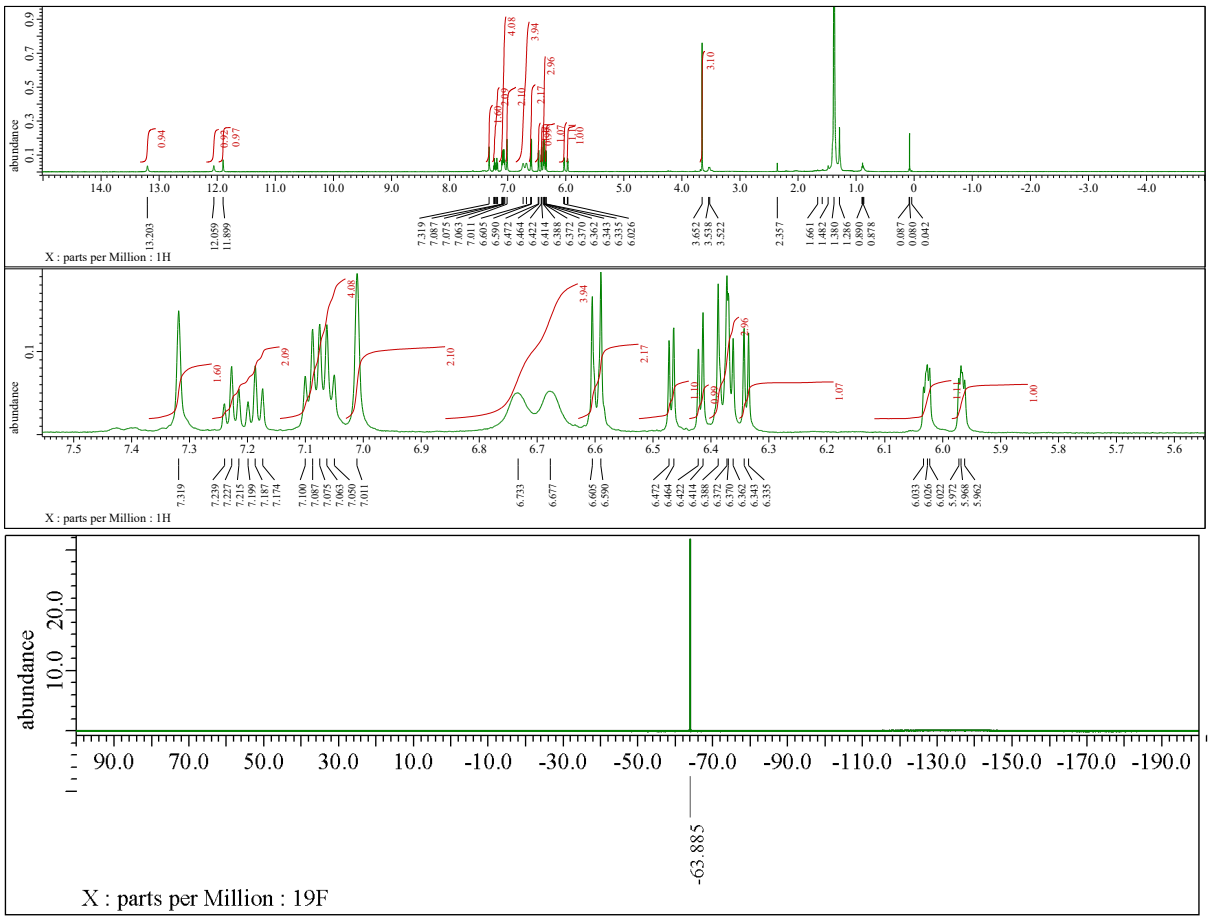

Figure S2-5. ^{1}H and ^{19}F NMR spectra of **2a** in cyclohexane-d_{12} at 25 °C.

Compound data of **2a** in cyclohexane-d_{12} at 25 °C
^{1}H-NMR (600 MHz, cyclohexane-d_{12}) δ 13.20 (s, 2H, NH), 12.06 (s, 2H, NH), 11.90 (s, 2H, NH), 7.32 (s, 2H, Ar-H), 7.24-7.17 (m, 4H, Ph), 7.07 (m, 8H, Ph), 7.01 (s, 4H, Ar-H), 6.80-6.63 (br, 8H, Ph), 6.60 (d, J = 9.0 Hz, 4H, MeO-C$_6$H$_4$), 6.47 (d, J = 5.0 Hz, 2H, β-H), 6.42 (d, J = 5.0 Hz, 2H, β-H), 6.39-6.36 (m, 6H, MeO-C$_6$H$_4$+β-H), 6.34 (d, J = 4.6 Hz, 2H, β-H), 6.03 (m, 2H, β-H), 5.97 (m, 2H, β-H) and 3.65 (s, 6H, OCH$_3$) ppm; ^{19}F-NMR (565 MHz, cyclohexane-d_{12}) δ –63.9 ppm

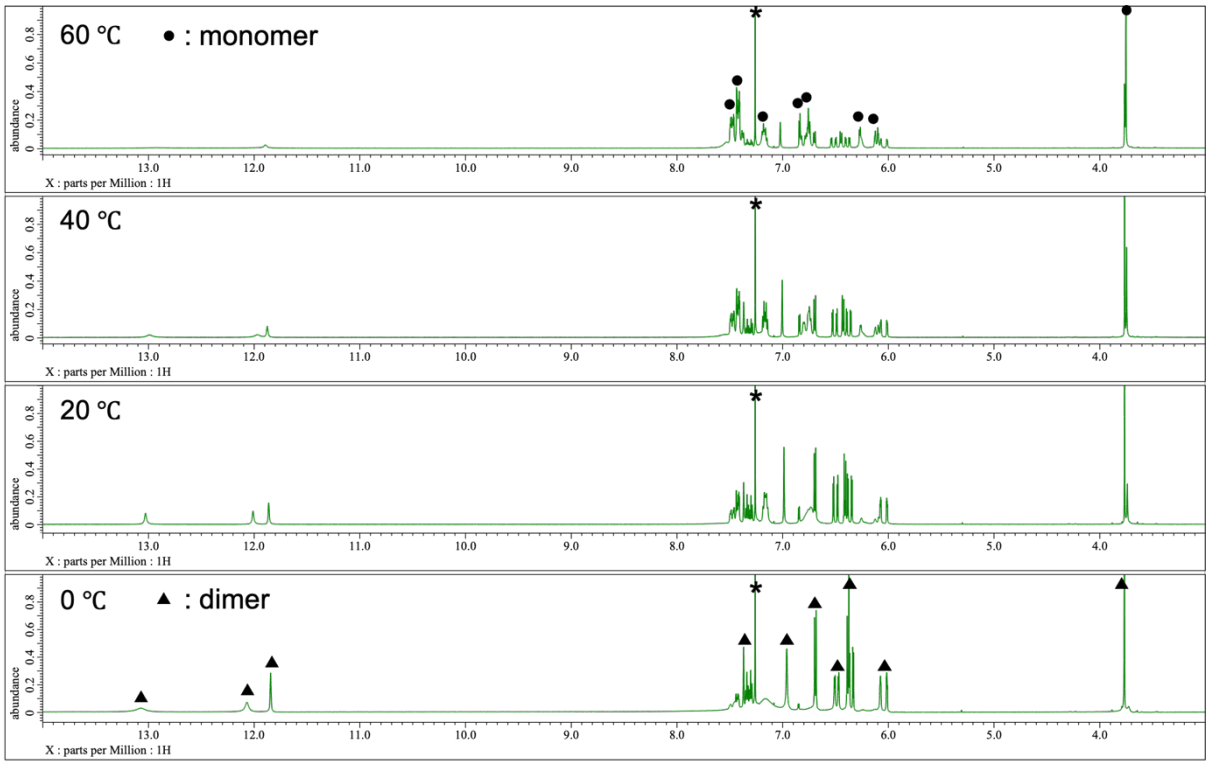

T/K	Monomer/mM	Dimer/mM	K_{dim}/M^{-1}	lnK_{dim}
273	1.42	4.29	2120	7.66
283	2.21	3.89	795.5	6.68
293	2.70	3.65	498.9	6.21
298	2.76	3.62	475.8	6.16
303	3.39	3.30	287.2	5.66
308	3.91	3.05	199.4	5.30
313	4.50	2.75	135.5	4.91
318	5.21	2.40	88.24	4.48
323	5.76	2.12	63.97	4.16
328	6.15	1.92	50.81	3.93
333	6.85	1.58	33.60	3.51

$$K_{dim} = \frac{[dimer]}{[monomer]^2}$$

van't Hoff equation

$$lnK_{dim} = -\frac{\Delta H}{RT} + \frac{\Delta S}{R}$$

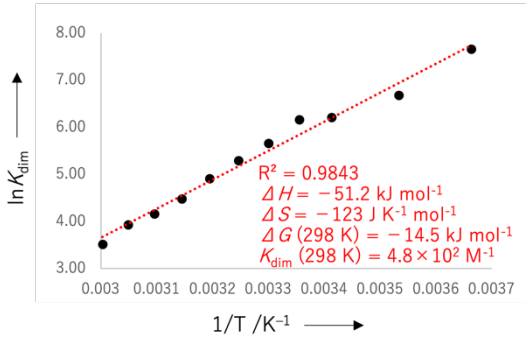

Figure S2-6. ^{1}H NMR spectra of **2a** at different temperatures in $CDCl_3$ and the van't Hoff plot for **2a**. *Solvent and impurities.

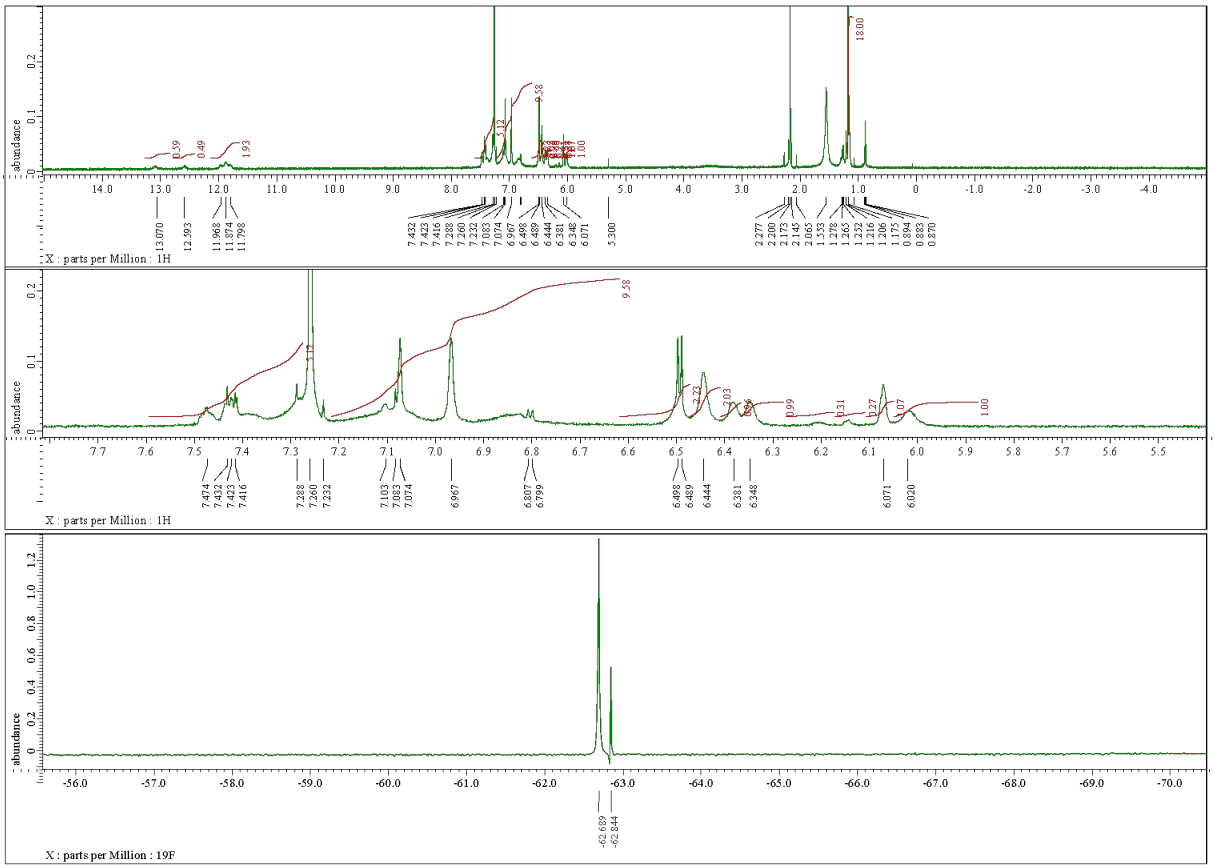

Figure S2-7. ^{1}H and ^{19}F NMR spectra of **2b** in $CDCl_3$ at 30 °C.

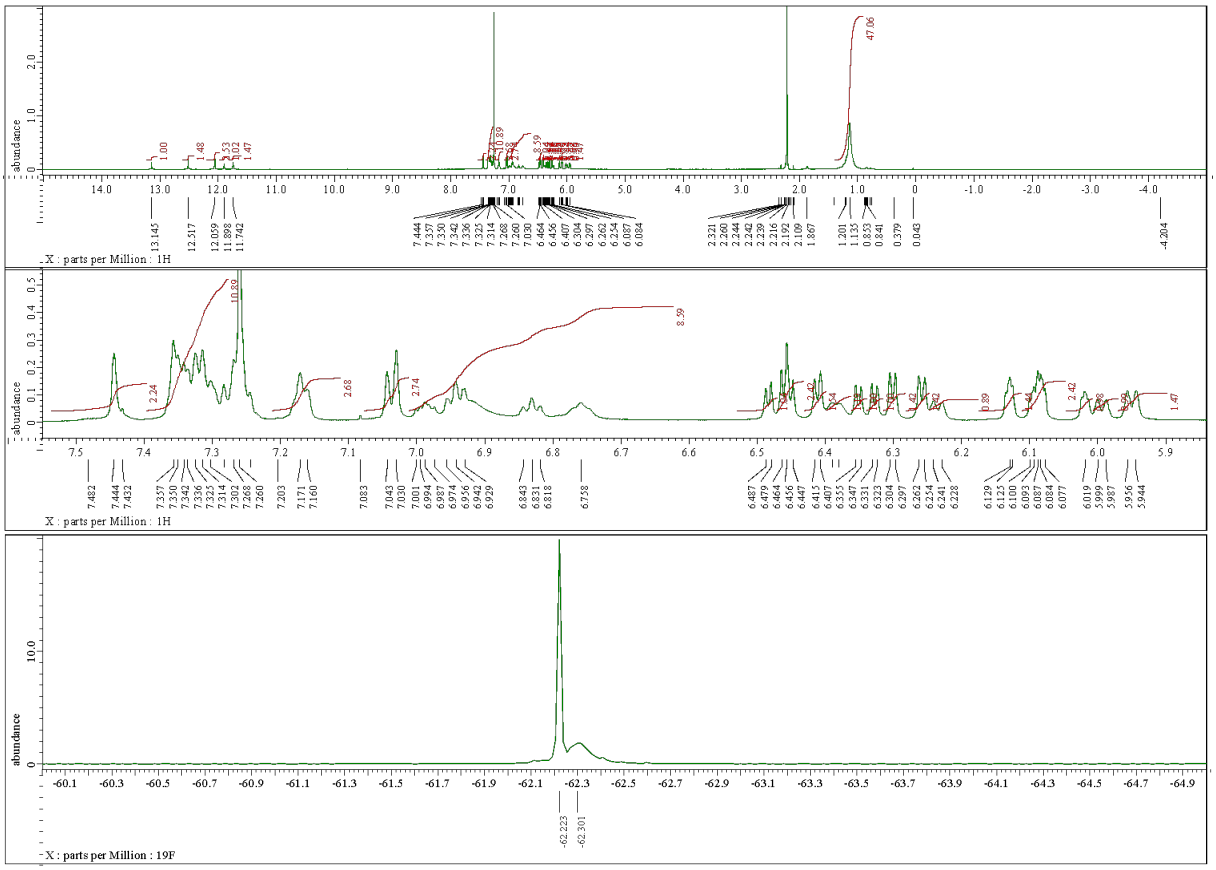

Figure S2-8. ^{1}H and ^{19}F NMR spectra of **2b** in $CDCl_3$ at –60 °C.

Compound data of **2b** in $CDCl_3$ at –60 °C

^{1}H-NMR (600 MHz, $CDCl_3$) δ 13.14, 12.52, 12.06, 11.90, 11.74, 7.43, 7.36-7.28, 7.17, 7.04, 6.99, 6.94, 6.83, 6.76, 6.48, 6.46, 6.41, 6.39, 6.35, 6.33, 6.30, 6.26, 6.23, 6.13, 6.08, 6.02, 5.99, 5.95, and 1.21-1.13 ppm

^{19}F-NMR (565 MHz, $CDCl_3$) δ –62.2 and –62.3 ppm

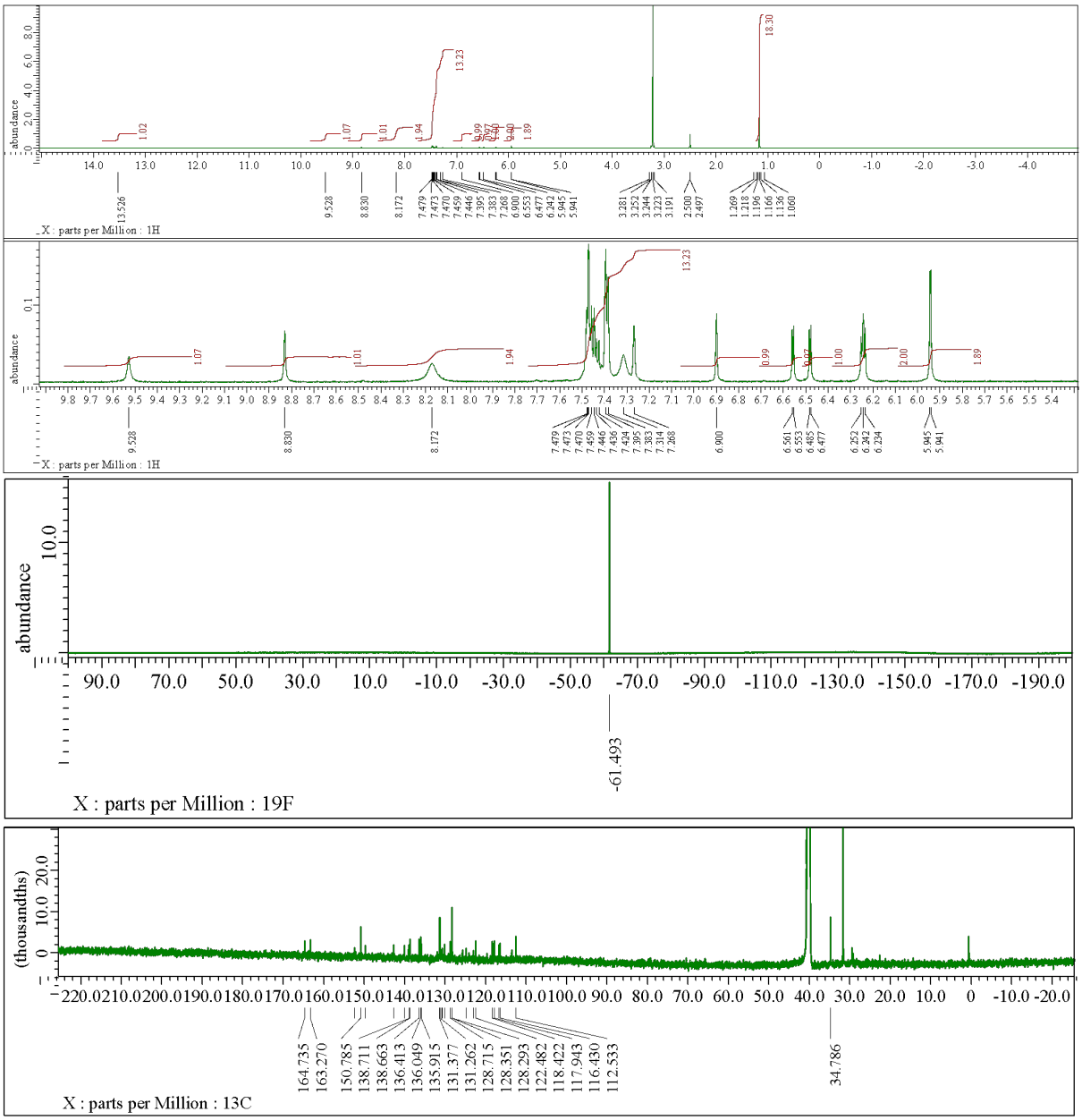

Figure S2-9. ^{1}H, ^{19}F and ^{13}C NMR spectra of **2b** in DMSO-d_6 at 50 °C.

Compound data of **2b** in DMSO-d_6 at 50 °C

^{1}H-NMR (600 MHz, DMSO-d_6) δ 13.53 (s, 1H, NH), 9.53 (s, 1H, NH), 8.83 (s, 1H, NH), 8.17 (s, 2H, Ar-H), 7.48-7.42 (m, 10H, Ph-H), 7.31 (s, 2H, Ar-H), 7.27 (s, 1H, Ar-H), 6.90 (s, 1H, Ar-H), 6.56 (d, J = 4.6 Hz, 1H, β-H), 6.48 (d, J = 4.6 Hz, 1H, β-H), 6.24 (m, 2H, β-H), 5.95 (d, J = 2.4 Hz, 2H, β-H) and 1.22-1.14 (m, 18H, *t*Bu-H) ppm; ^{19}F-NMR (565 MHz, DMSO-d_6) δ –61.5 ppm; ^{13}C-NMR (151 MHz, DMSO-d_6) δ 164.7, 163.3, 152.4, 150.8, 149.7, 142.7, 140.1, 139.0, 138.7, 138.7, 136.4, 136.0, 135.9, 131.4, 131.3, 130.9, 130.7, 130.1, 128.7, 128.4, 128.3, 124.9, 123.1, 122.5, 118.4, 117.9, 116.8, 116.4, 112.5 and 34.8 ppm

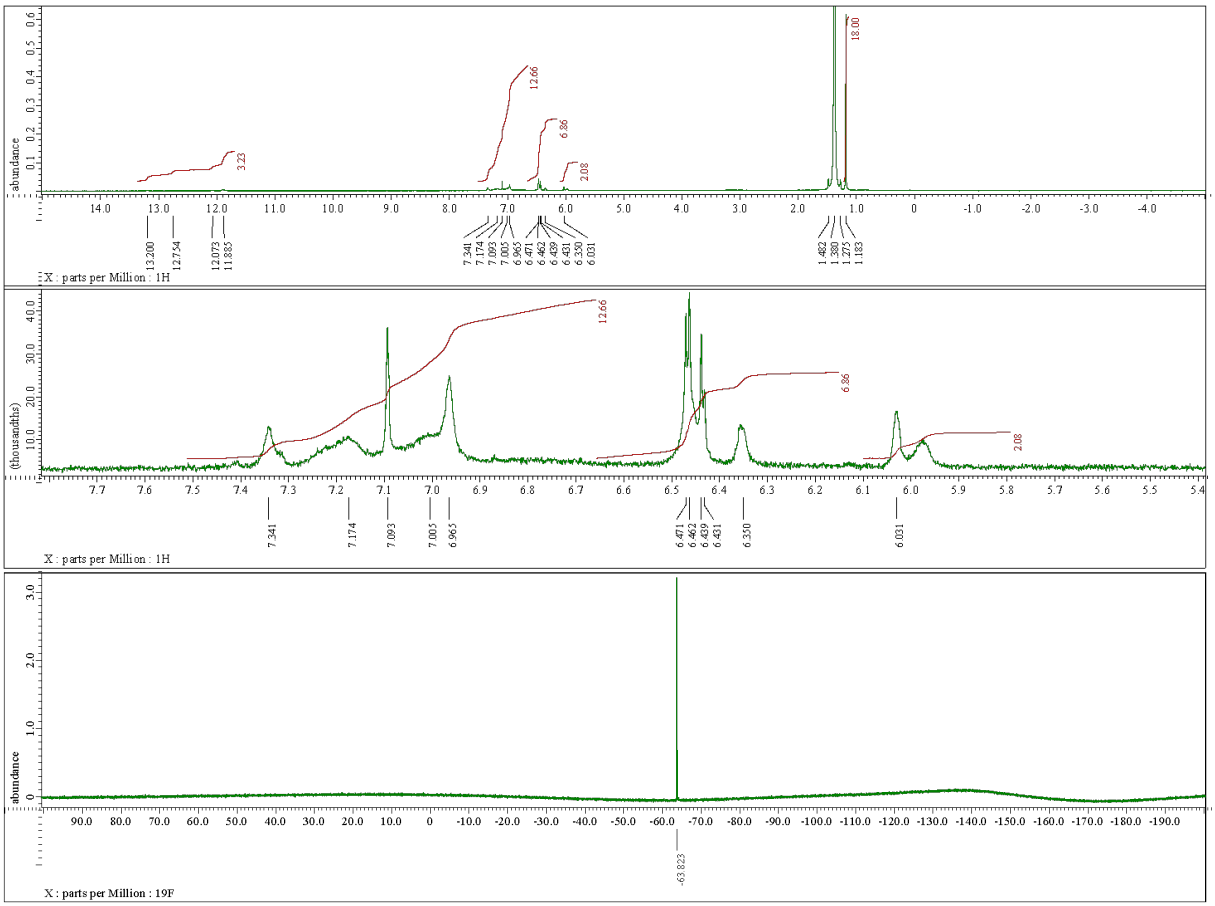

Figure S2-10. ^{1}H and ^{19}F NMR spectra of **2b** in cyclohexane-d_{12} at 25 °C.

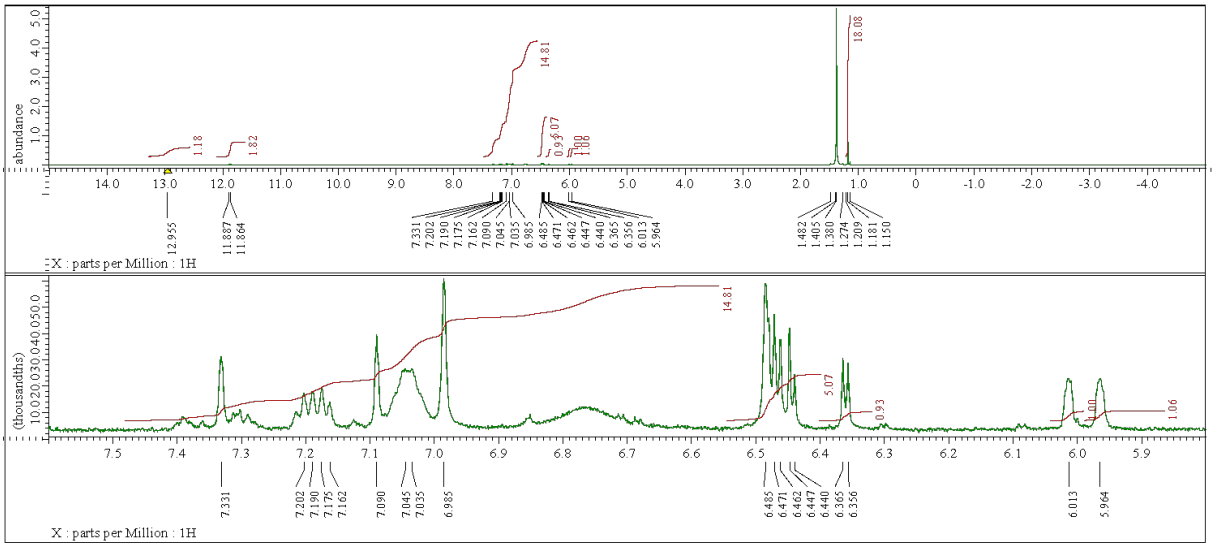

Figure S2-11. ^{1}H NMR spectrum of **2b** in cyclohexane-d_{12} at 50 °C.

Compound data of **2b** in cyclohexane-d_{12} at 50 °C

^{1}H-NMR (600 MHz, cyclohexane-d_{12}) δ 12.96 (s, 2H, NH), 11.89 (s, 2H, NH), 11.86 (s, 2H, NH), 7.33 (s, 2H, Ar-H), 7.19 (m, 4H, Ph-H), 7.09 (s, 2H, Ar-H), 7.08-7.00 (br, 8H, Ph-H), 6.99 (s, 4H, Ar-H), 6.88-6.65 (br, 8H, Ph), 6.48-6.44 (m, 10H, Ar-H+β-H), 6.36 (d, J = 5.0 Hz, 2H, β-H), 6.01 (s, 2H, β-H), 5.96 (s, 2H, β-H) and 1.21-1.15 (m, 36H, tBu-H) ppm

Compound data of **2b** in cyclohexane-d_{12} at 25 °C

^{19}F-NMR (565 MHz, cyclohexane-d_{12}) δ = –63.8 ppm

(a)

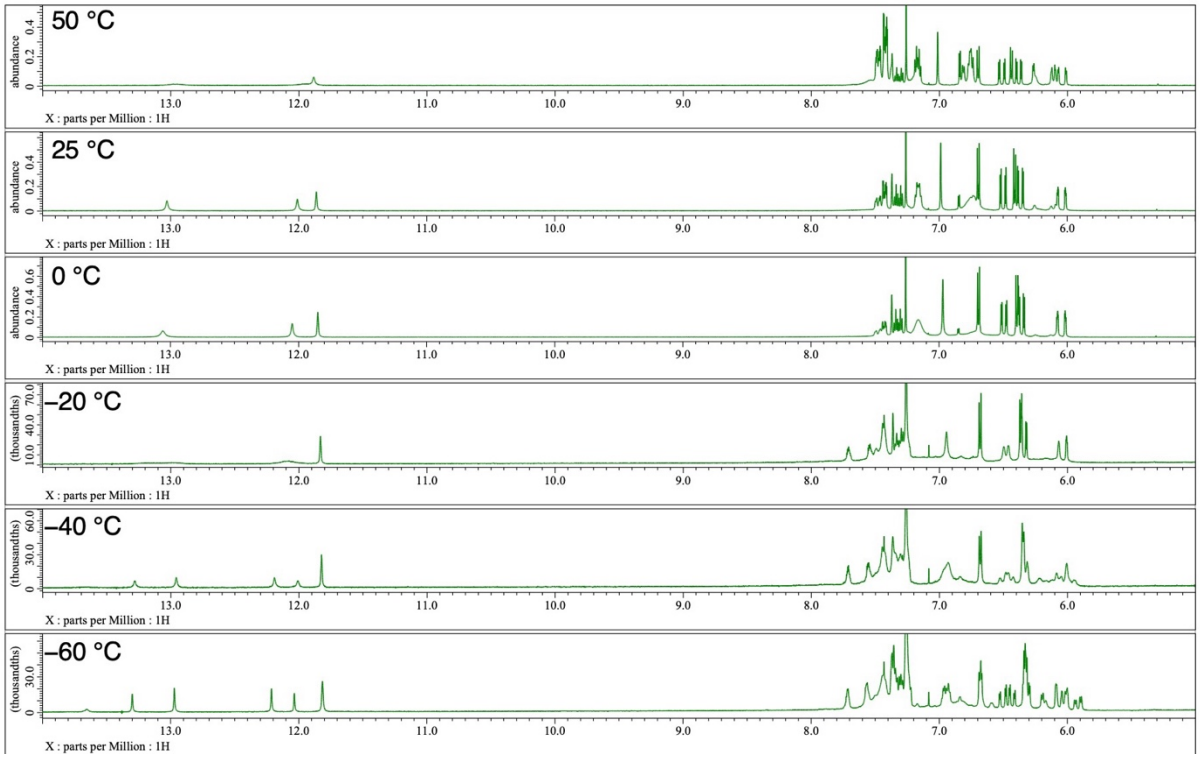

(b)

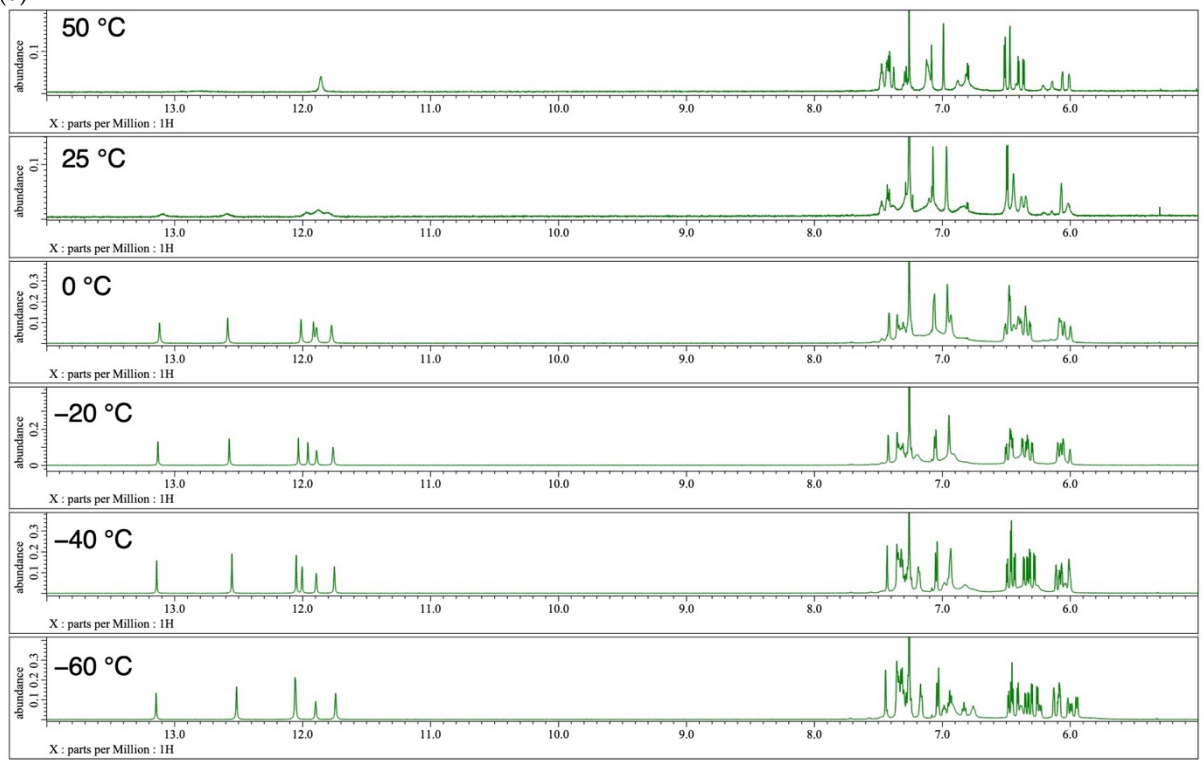

Figure S2-12. Variable-temperature ^{1}H NMR spectra of (a) **2a** and (b) **2b** in $CDCl_3$.

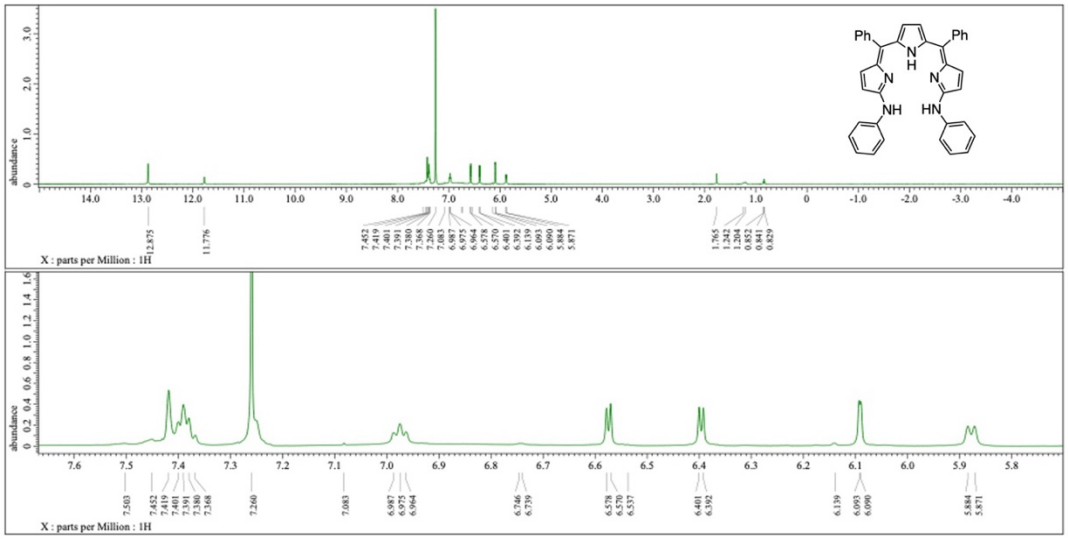

Figure S2-13. ^{1}H NMR spectrum of α,α'-dianilinotripyrrin in $CDCl_3$ at –60 °C.[S4]

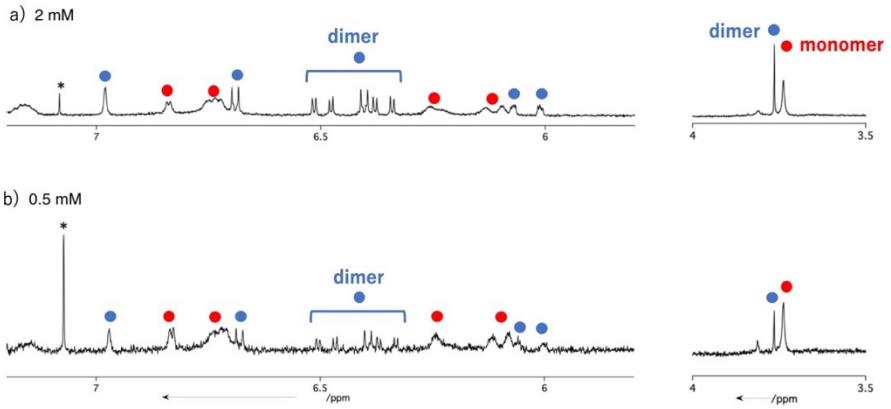

Figure S2-14. Concentration-dependence of the ^{1}H NMR spectra of **2a** in $CDCl_3$ at room temperature. a) 2 mM and b) 0.5 mM. Selected regions are shown.

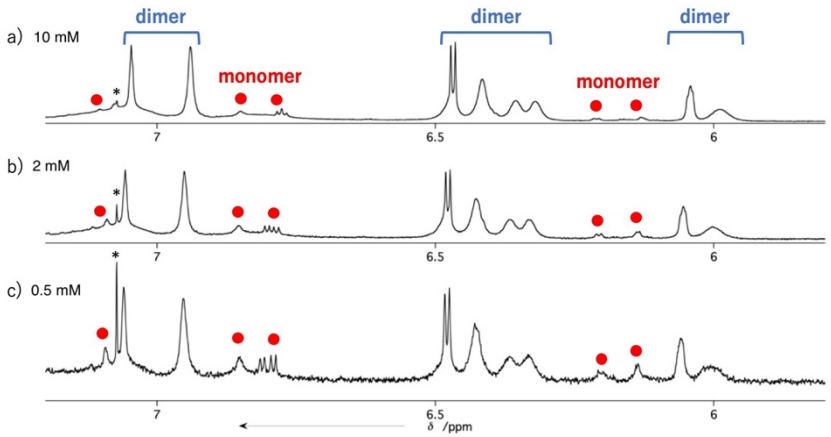

Figure S2-15. Concentration-dependence of the ^{1}H NMR spectra of **2b** in $CDCl_3$ at room temperature. a) 10 mM, b) 2 mM and c) 0.5 mM. Selected regions are shown.

3. Mass Spectra

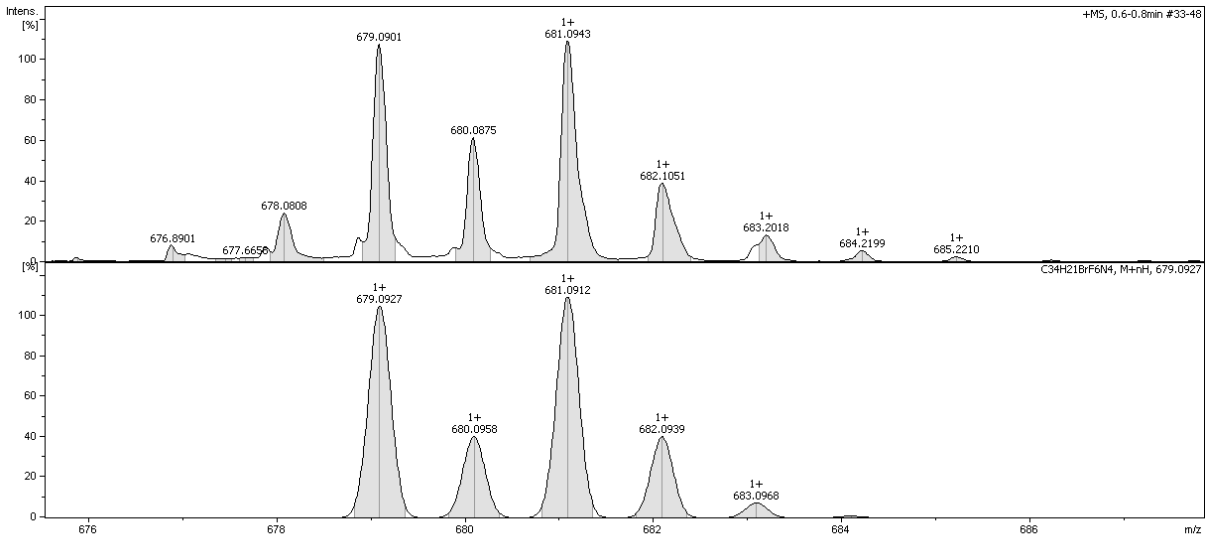

Figure S3-1. Observed (top) and simulated (bottom) HR-APCI-TOF mass spectra of **4**.

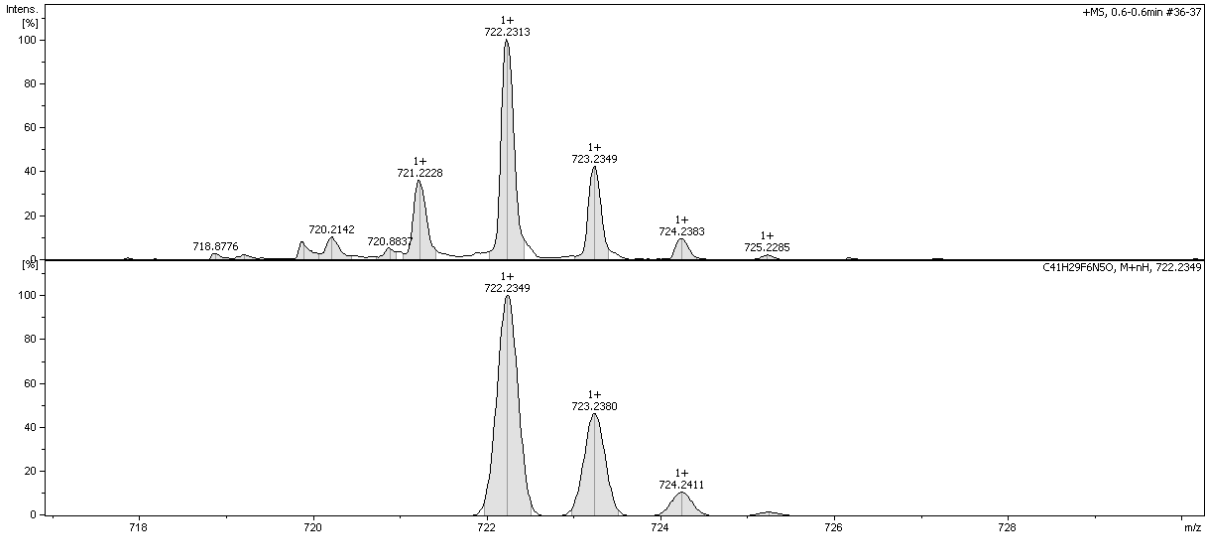

Figure S3-2. Observed (top) and simulated (bottom) HR-APCI-TOF mass spectra of **2a**.

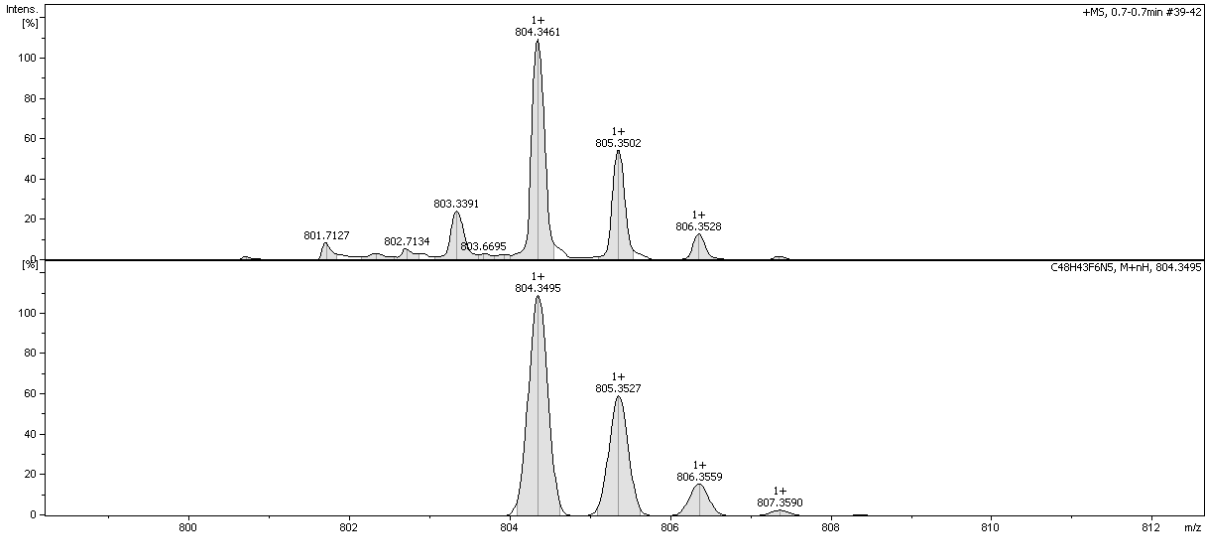

Figure S3-3. Observed (top) and simulated (bottom) HR-APCI-TOF mass spectra of **2b**

4. Optimization of the Acid-mediated Substitution Reactions

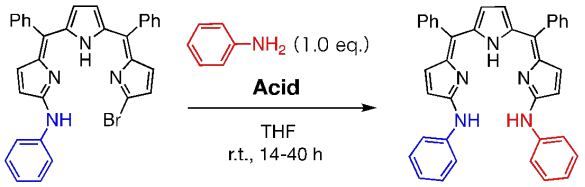

entry	**Acid**	NMR yields
1	CH_3COOH (1.0 eq.)	No Reaction
2	TFA (1.0 eq.)	42% (47% recovery)
3	TFA (2.0 eq.)	74% (7% recovery)
4	$MeSO_3H$ (1.0 eq.)	65% (14% recovery)
5	$MeSO_3H$ (2.0 eq.)	73% (12% recovery)

Table S4-1. Acid-mediated nucleophilic substitution reactions of 1-anilino-14-bromo-5,10-diphenyltripyrrin with aniline.

5. X-Ray Crystallographic Details

Table S5-1. Crystal data and structure refinements for **2a** and **2b**.

Compound	**2a**	**2b**
Empirical Formula	$C_{41}H_{29}F_6N_5O \cdot CH_2Cl_2$	$C_{48}H_{43}F_6N_5 \cdot C_6H_{14}$
M_W	806.62	890.05
Crystal System	monoclinic	triclinic
Space Group	*C*2/*c* (No. 15)	*P*-1 (No. 2)
a [Å]	28.6554(4)	14.7295(1)
b [Å]	15.7158(3)	15.7269(1)
c [Å]	16.5684(2)	22.3191(2)
α[deg]	90	108.0093(6)
β [deg]	91.5490(10)	104.2933(6)
γ [deg]	90	93.4445(6)
Volume [Å^3]	7458.73(17)	4712.20(6)
Z	8	2
Density [g/cm^3]	1.437	1.255
Completeness	0.995	0.952
Goodness-of-fit	1.102	1.031
R_1 [$I > 2\sigma(I)$]	0.0699	0.0477
wR_2 (all data)	0.2104	0.1274
Solvent System	CH_2Cl_2/*n*-hexane	THF/*n*-hexane
CCDC No.	2192332	2192331

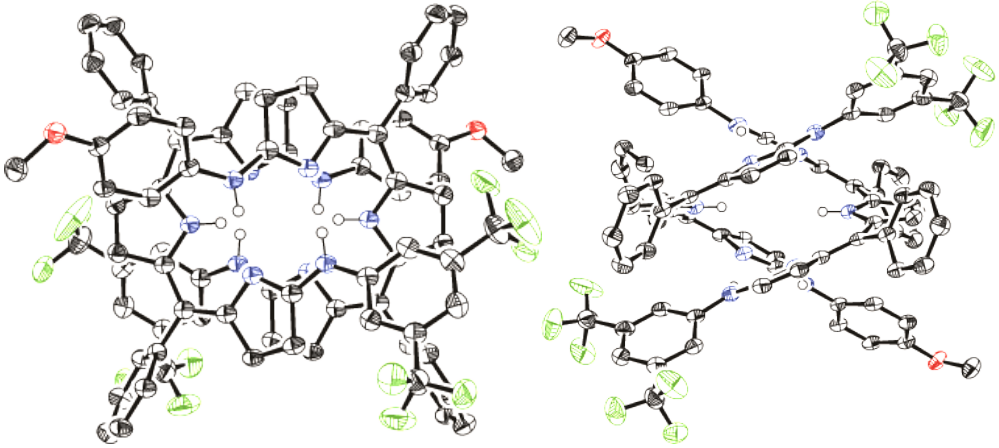

Figure S5-1. X-Ray structure of **2a**; (left) Top view and (right) side view. Thermal ellipsoids are shown at the 50% probability level. Hydrogen atoms except for NHs were omitted.

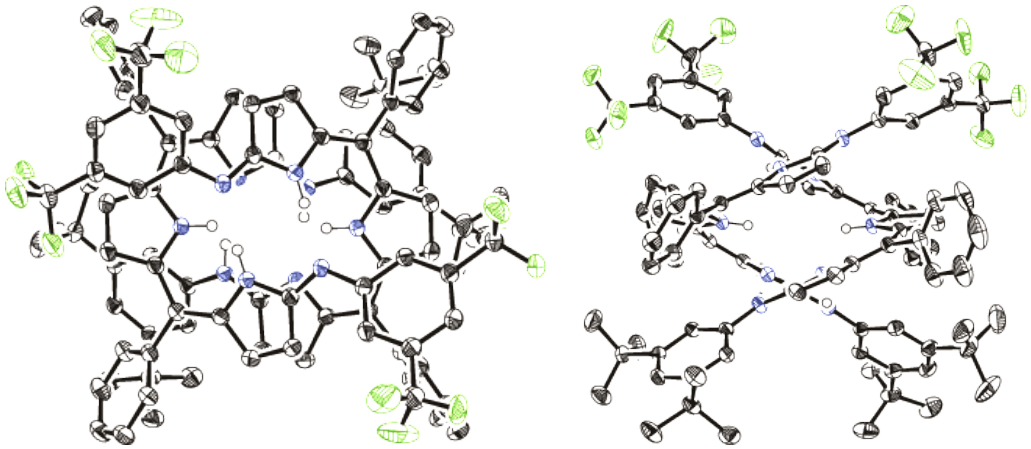

Figure S5-2. X-Ray structure of **2b**; (left) Top view and (right) side view. Thermal ellipsoids are shown at the 50% probability level. Hydrogen atoms except for NHs were omitted.

6. DFT Calculations

Geometry optimization and frequency calculations were carried out using the Gaussian 16 program.[S3] All structures were fully optimized without any symmetry restriction. The calculations were performed by the density functional theory (DFT) method with restricted B3LYP (Becke's three-parameter hybrid exchange functionals and the Lee-Yang-Parr correlation functional) level,[S5] employing basis sets 6-311G++(d,p) or def2-SVP for all atoms, and the D3 version of Grimme's dispersion with Becke–Johnson damping.[S6] Solvation effect of chloroform was modeled by SMD method.[S7]

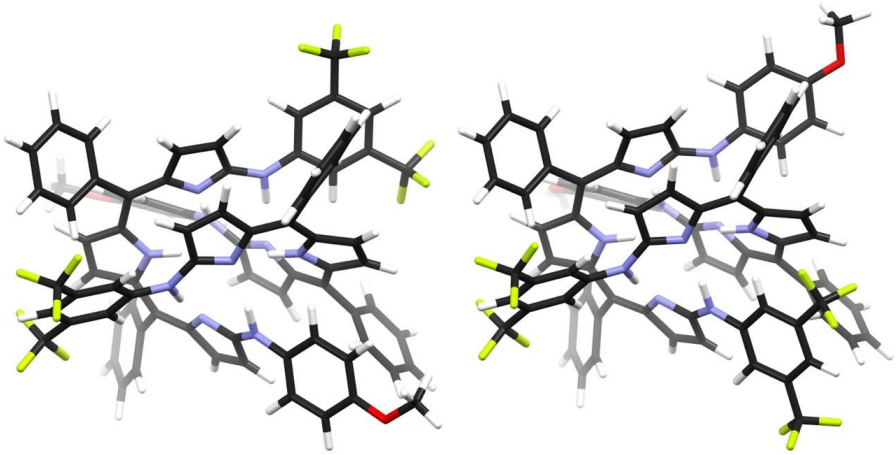

Figure S6-1. Optimized structures of **2a**; (left) *anti*-type, (right) *syn*-type. The structures were calculated at the B3LYP-D3BJ/6-311G++(d,p) level based on the crystal structure by changing aryl substituents.

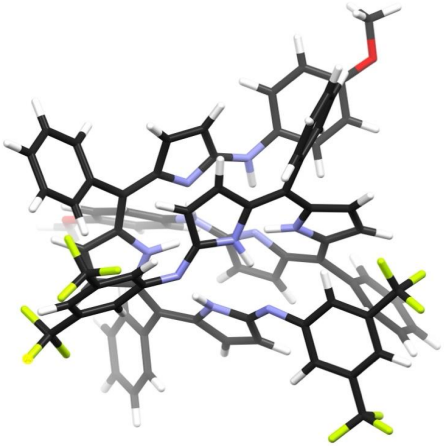

Figure S6-2. Optimized structure of the NH-tautomer of **2a**; *syn*-type. The structure was calculated at the B3LYP-D3BJ/6-311G++(d,p) level based on the crystal structure of **2b** by changing aryl substituents.

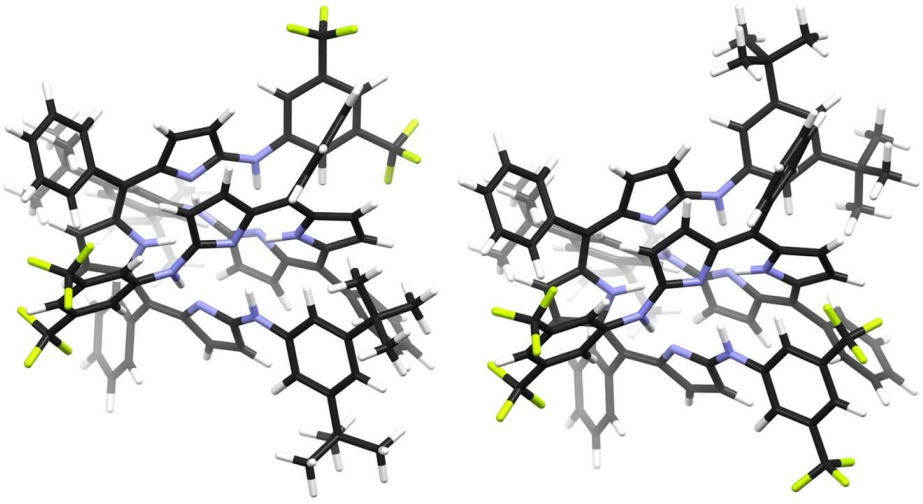

Figure S6-3. Optimized structures of **2b**; (left) *anti*-type, (right) *syn*-type. The structures were calculated at the B3LYP-D3BJ/6-311G++(d,p) level based on the crystal structure of **2a** by changing aryl substituents.

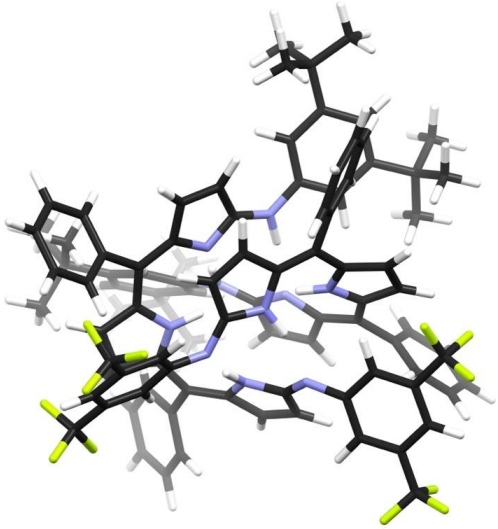

Figure S6-4. Optimized structure of the NH-tautomer of **2b**; *syn*-type. The structure was calculated at the B3LYP-D3BJ/6-311G++(d,p) level based on the crystal structure.

Table S6-1. Comparison of the calculated and relative energies for the different conformers of **2a** and **2b**. calculated at the B3LYP-D3BJ/6-311++G(d,p) level.

2a	**2a-*anti***	**2a-*syn***	**2a′-*syn***
Electronic and thermal energy	–5056.286677 hartree	–5056.285310 hartree	–5056.285326 hartree
	0 kJ/mol	+3.589 kJ/mol	+3.547 kJ/mol
Electronic and thermal enthalpy	–5056.285733 hartree	–5056.284365 hartree	–5056.284382 hartree
	0 kJ/mol	+3.592 kJ/mol	+3.547 kJ/mol
Electronic and thermal free energy	–5056.510008 hartree	–5056.508901 hartree	–5056.509291 hartree
	0 kJ/mol	+2.906 kJ/mol	+1.882 kJ/mol
Total energy	–5057.612502 hartree	–5057.611160 hartree	–5057.610602 hartree
	0 kJ/mol	+3.523 kJ/mol	+4.988 kJ/mol

2b	**2b-*anti***	**2b-*syn***	**2b′-*syn***
Electronic and thermal energy	–5456.060280 hartree	–5456.060096 hartree	–5456.060906 hartree
	+1.644 kJ/mol	2.127 kJ/mol	0 kJ/mol
Electronic and thermal enthalpy	–5456.059336 hartree	–5456.059152 hartree	–5456.059962 hartree
	+1.644 kJ/mol	2.127 kJ/mol	0 kJ/mol
Electronic and thermal free energy	–5456.319108 hartree	–5456.318905 hartree	–5456.318159 hartree
	0 kJ/mol	+0.533 kJ/mol	+2.492 kJ/mol
Total energy	–5457.786700 hartree	–5457.786486 hartree	–5457.786989 hartree
	+0.759 kJ/mol	+1.321 kJ/mol	0 kJ/mol

Table S6-2. Comparison of the calculated and relative energies for the different conformers of **2a** and **2b**. calculated at the B3LYP-D3BJ/def2-SVP/SMD($CHCl_3$) level.

2a	**2a-*anti***	**2a-*syn***	**2a′-*syn***
Electronic and thermal energy	–5051.562867 hartree	–5051.562309 hartree	–5051.560476 hartree
	0 kJ/mol	+1.465 kJ/mol	+6.278 kJ/mol
Electronic and thermal enthalpy	–5051.342041 hartree	–5051.341275 hartree	–5051.340674 hartree
	0 kJ/mol	+2.011 kJ/mol	+3.589 kJ/mol
Electronic and thermal free energy	–5051.342985 hartree	–5051.342219 hartree	–5051.341618 hartree
	0 kJ/mol	+2.011 kJ/mol	+3.589 kJ/mol
Total energy	–5052.675278 hartree	–5052.674165 hartree	–5052.672854 hartree
	0 kJ/mol	+2.922 kJ/mol	+6.364 kJ/mol

2b	**2b-*anti***	**2b-*syn***	**2b′-*syn***
Electronic and thermal energy	–5450.736852 hartree	–5450.737615 hartree	–5450.736772 hartree
	+2.003 kJ/mol	0 kJ/mol	+2.213 kJ/mol
Electronic and thermal enthalpy	–5450.735908 hartree	–5450.736671 hartree	–5450.735828 hartree
	+2.003 kJ/mol	0 kJ/mol	+2.213 kJ/mol
Electronic and thermal free energy	–5450.993345 hartree	–5450.988843 hartree	–5450.990403 hartree
	0 kJ/mol	+11.820 kJ/mol	+7.723 kJ/mol
Total energy	–5452.468190 hartree	–5452.467603 hartree	–5452.467255 hartree
	+0 kJ/mol	+1.541 kJ/mol	+2.455 kJ/mol

Table S6-3. Comparison of the calculated and relative energies for the different conformers of symmetric dianilinotripyrrin. calculated at the B3LYP-D3BJ/6-311++G(d,p) level (top) and B3LYP-D3BJ/def2-SVP/SMD($CHCl_3$) level (bottom).

B3LYP-D3BJ/6-311++G(d,p)	*symm-*	*taut-*
Electronic and thermal energy	–3478.631188 hartree	–3478.628494 hartree
	0 kJ/mol	7.073 kJ/mol
Electronic and thermal enthalpy	–3478.630244 hartree	–3478.627550 hartree
	0 kJ/mol	+7.073 kJ/mol
Electronic and thermal free energy	–3478.804153 hartree	–3478.801580 hartree
	0 kJ/mol	+6.755 kJ/mol
Total energy	–3479.854945 hartree	–3479.851733 hartree
	0 kJ/mol	+8.433 kJ/mol

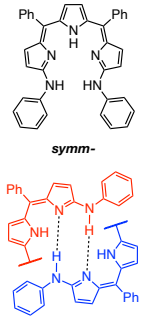

B3LYP-D3BJ/def2-SVP/SMD($CHCl_3$)	*symm-*	*taut-*
Electronic and thermal energy	–3475.371009 hartree	–3475.367183 hartree
	0 kJ/mol	+10.045 kJ/mol
Electronic and thermal enthalpy	–3475.370065 hartree	–3475.367183 hartree
	0 kJ/mol	+7.567 kJ/mol
Electronic and thermal free energy	–3475.542693 hartree	–3475.540409 hartree
	0 kJ/mol	+5.997 kJ/mol
Total energy	–3476.599293 hartree	–3476.595761 hartree
	0 kJ/mol	+9.273 kJ/mol

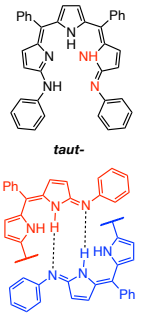

7. UV/Vis Absorption Spectra

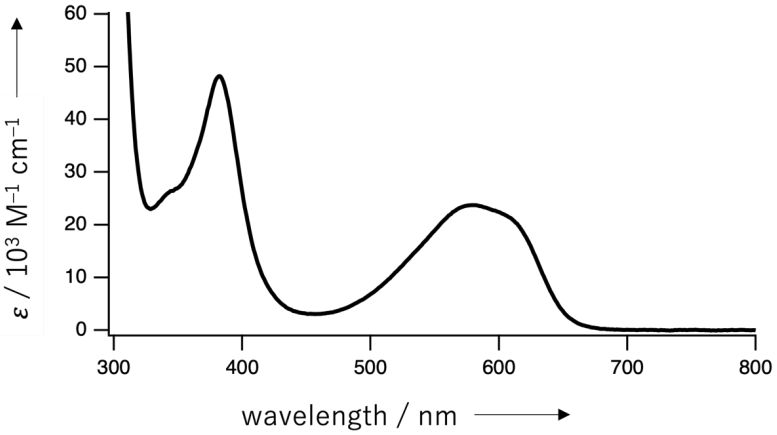

Figure S7-1. UV/Vis absorption spectrum of **4** in CH_2Cl_2.
UV/Vis (CH_2Cl_2) λ_{max} (ε / 10^4 M^{-1} cm^{-1}) = 382 (4.8) and 579 (2.4) nm.

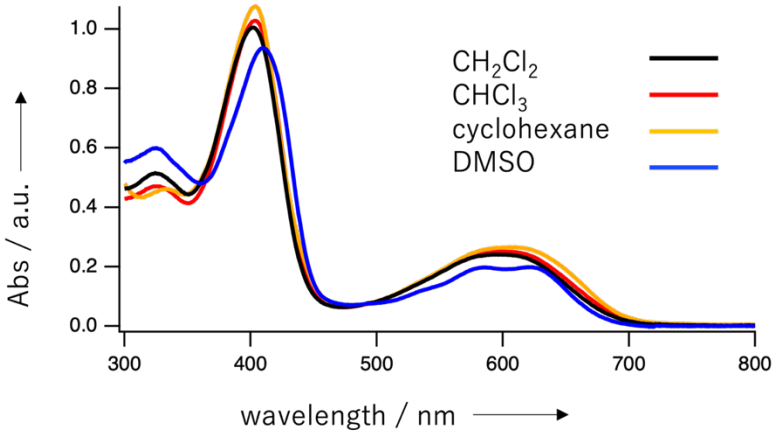

Figure S7-2. UV/Vis absorption spectra of **2a** in several solvents.

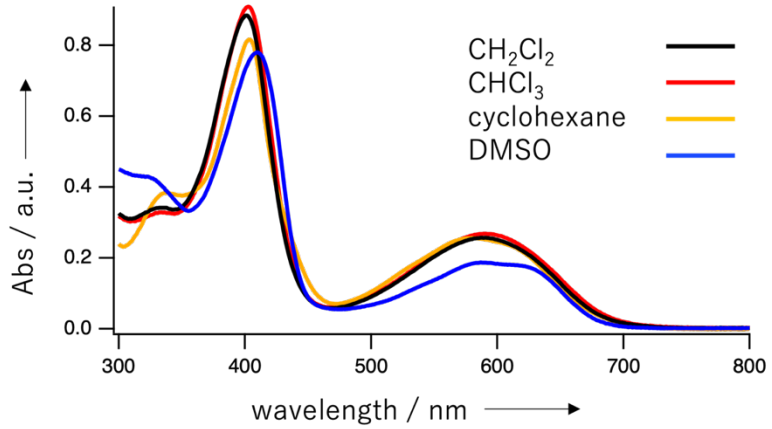

Figure S7-3. UV/Vis absorption spectra of **2b** in several solvents.

8. Supporting References

[S1] G. M. Sheldrick, *Acta Cryst*., 2015, **A71**, 3.

[S2] a) G. M. Sheldrick and T. R. Schneider, *Methods Enzymol.,* 1997, **277**, 319; b) G. M. Sheldrick, *Acta Cryst*., 2015, **C71**, 3.

[S3] Gaussian 16, Revision B.01, M. J. Frisch, G. W. Trucks, H. B. Schlegel, G. E. Scuseria, M. A. Robb, J. R. Cheeseman, G. Scalmani, V. Barone, G. A. Petersson, H. Nakatsuji, X. Li, M. Caricato, A. V. Marenich, J. Bloino, B. G. Janesko, R. Gomperts, B. Mennucci, H. P. Hratchian, J. V. Ortiz, A. F. Izmaylov, J. L. Sonnenberg, D. Williams-Young, F. Ding, F. Lipparini, F. Egidi, J. Goings, B. Peng, A. Petrone, T. Henderson, D. Ranasinghe, V. G. Zakrzewski, J. Gao, N. Rega, G. Zheng, W. Liang, M. Hada, M. Ehara, K. Toyota, R. Fukuda, J. Hasegawa, M. Ishida, T. Nakajima, Y. Honda, O. Kitao, H. Nakai, T. Vreven, K. Throssell, J. A. Montgomery, Jr., J. E. Peralta, F. Ogliaro, M. J. Bearpark, J. J. Heyd, E. N. Brothers, K. N. Kudin, V. N. Staroverov, T. A. Keith, R. Kobayashi, J. Normand, K. Raghavachari, A. P. Rendell, J. C. Burant, S. S. Iyengar, J. Tomasi, M. Cossi, J. M. Millam, M. Klene, C. Adamo, R. Cammi, J. W. Ochterski, R. L. Martin, K. Morokuma, O. Farkas, J. B. Foresman and D. J. Fox, Gaussian, Inc., Wallingford CT, 2016.

[S4] M. Umetani, T. Tanaka and A. Osuka, *Chem. Sci*., 2018, **9**, 6853.

[S5] a) C. Lee, W. Yang and R. G. Parr, *Phys. Rev. B*, 1988, **37**, 785; b) A. D. Becke, *J. Chem. Phys*., 1993, **98**, 1372.

[S6] Empirical dispertion, D3(BJ): a) S. Grimme, J. Antony, S. Ehrlich, H. Krieg, *J. Chem. Phys*. **2010**, *132*, 154104; b) S. Grimme, S. Ehrlich, L. Goerigk, *J. Comput. Chem*. **2011**, *32*, 1456.

[S7] A. V. Marenich, C. J. Cramer and D. G. Truhlar, *J. Phys. Chem. B*., 2009, **113**, 6378.